Composites: Part A 84 (2016) 103–113

Contents lists available at ScienceDirect

Composites: Part A

journal homepage: www.elsevier.com/locate/compositesa

Matrix failure in composite laminates under compressive loading

Nayeem Tawqir Chowdhury [a,*], John Wang [b], Wing Kong Chiu [a], Wenyi Yan [a]

[a] Department of Mechanical and Aerospace Engineering, Monash University, Clayton, VIC 3800, Australia
[b] Aerospace Division, Defence Science and Technology Group, 506 Lorimer St., Fishermans Bend, Vic. 3207, Australia

ARTICLE INFO

Article history:
Received 11 July 2015
Received in revised form 8 January 2016
Accepted 11 January 2016
Available online 18 January 2016

Keywords:
A. Polymer-matrix composites (PMCs)
A. Resins
D. Mechanical testing
Microstructural analysis

ABSTRACT

The failure envelope of the matrix in composite laminates under compressive loads has not received much attention in literature. There are very little to no experimental results to show a suitable failure envelope for this constituent found in composites. With increasing popularity in the use of micromechanical analysis to predict progressive damage of composite structures which requires the use of individual failure criteria for the fibre and matrix, it is important that matrix behaviour under compression is modelled correctly.

In this study, off-axis compression tests under uniaxial compression loading are used to promote matrix failure. Through the use of micromechanical analysis involving Representative Volume Elements, the authors were able to extract the principal stresses on the matrix at failure. The results indicated that hydrostatic stresses play an important role in the failure of the matrix. Thus, Drucker–Prager failure criterion is recommended when modelling compressive matrix failure in composite structures.

Crown Copyright © 2016 Published by Elsevier Ltd. All rights reserved.

1. Introduction

Fibre reinforced polymer materials commonly known as composites are increasingly being used due to their high strength to weight ratio and high fatigue resistance. In order to ensure structural integrity of the components which they form, it is important to understand their behaviour at failure. However as failure in composites are characterised by different modes, namely fibre, matrix and interfacial failure [1], this has complicated the understanding of the failure behaviour. For this reason there are still many unanswered questions as to the materials' failure characteristics, one of which includes matrix compression failure.

In an ideal situation, a composite would be modelled with each strand of fibre surrounded by a polymeric matrix. This would allow for the stress and strain states of the fibre, matrix and interface to be extracted separately. However, this is obviously computationally prohibitive. One method that has greatly assisted in simplifying this analysis is Classical Laminate Theory (or CLT) [2]. This theory combines the properties of the fibre and the matrix through an averaging approach to form what is considered to be a new homogenous material called a lamina. CLT is widely used by researchers in the field and given its simplicity, it does a good job at modelling the stiffness of a laminate including linear load behaviour up to the point of failure. One improvement that can be made to this theory would be the ability to separately examine the fibre and the matrix. This can be done using micromechanical analysis.

For failure assessment, micromechanical analysis can be used to separate the stress–strain states in the matrix and fibre components from a Representative Volume Element (or RVE). The relationship can then be used in a structural analysis to predict matrix or fibre failure. One popular analysis method that uses micromechanical analysis is Multicontinuum Theory (or MCT) [3,4]. MCT predicts failure at the fibre and matrix level by obtaining the volume averaged stress states in the fibre and the matrix. Here, matrix failure is assumed to be influenced by all six of the matrix average stress components in a 3D analysis, whilst a quadratic function is used to find the average stress of the fibre [3]. This particular theory greatly assists with understanding matrix failure and fibre failure in a composite, especially when it comes to progressive damage models [5–8]. However, the assumption of averaging the overall stresses in the individual constituents can be improved on. An analysis method that does this is the Amplification Technique [9–11]. Unlike MCT, where the stresses in each constituent are averaged, the amplification technique calculates the principal stresses and strains at several locations to identify a critical location. Using this separation technique allows the fibre and matrix failure to be examined in detail.

Fibre failure has been quite extensively researched in the field of composites, whilst at a micromechanical level, matrix failure has not received the same amount of attention. Matrix failure is typically known to take place well before the fibre in matrix

* Corresponding author.
E-mail address: nayeem.chowdhury@monash.edu (N.T. Chowdhury).

http://dx.doi.org/10.1016/j.compositesa.2016.01.007
1359-835X/Crown Copyright © 2016 Published by Elsevier Ltd. All rights reserved.

dominated load cases and can be characterised by three main modes; tension, compression and shear failure. Some authors have proposed these modes of failure to be characterised by dilatational failure and distortional failure [10,12]. In this paper the authors focus on distortional matrix failure in composites.

Matrix failure under tension loading has received some attention in literature. The most commonly known form of this test is the 10° off-axis tension test on a uniaxial composite to find the shear modulus of the lamina [13,14,15]. Others have also performed a range of off-axis tests on uniaxial composites where the fibre direction changes [14,15]. The authors have also explored this form of failure through several biaxial tension tests under different loading ratios [16,17]. Through the use of micromechanical analysis, some have proposed the tension quadrant of a principal stress based failure envelope to be truncated [9,10,16,17]. This idea is not new in the field of isotropic materials, where existing failure criteria have proposed this. The simplest example is maximum stress theory which predicts failure when the stress state in the material exceeds its tensile strength. Others include: Drucker–Prager, Mohr–Coulomb, and recently, SIFT (First Strain Invariant) or Onset Theory [18].

Unlike matrix tensile failure, there are few papers that explore shear and compression failure of the matrix at a micromechanics level. One of the few failure criteria that utilises micromechanical analysis to predict matrix failure is that proposed by Gosse and Christensen called Onset Theory [9,10]. Their criterion uses von Mises failure criterion to predict what they term as distortional failure of the matrix [9]. This implies that they consider both shear and compressive failure in composites to be modelled by von Mises. With the assumption that a matrix can be treated as an isotropic material, literature has shown that in the shear quadrants of a stress based material failure envelope, von Mises failure criterion does a good job in predicting failure [17]. However, it should be noted that von Mises theory does not consider hydrostatic stresses, which is known to play an important role in the failure of isotropic materials under compression. To account for this phenomenon, von Mises failure criterion was modified to account for hydrostatic stresses. One of these theories is Drucker–Prager failure criterion which has been quite successful in modelling shear and compression failure in monolithic isotropic materials [19]. Thus, the authors aim to perform a set of experiments using Classical Laminate Theory and micromechanical analysis to examine the importance of considering hydrostatic stresses when a matrix fails due to compression.

2. Uniaxial compression

2.1. Experiment methodology

There are three main types of antibuckling rigs used for compression tests: (1) the modified ASTM D 695 standard; (2) the IITRI compression test method; and (3) the combined loading test methods [20]. Out of the three test methods, the latter two have been shown to considerably reduce end crushing when compared to the modified ASTM D695 test method. This is due to the fixture's ability to transfer the loads through shear. In the case of the experiments considered in this study, the authors are interested in matrix failure, which occurs at much lower loads compared to layups examining fibre failure. Thus, end crushing is not as prominent in these set of experiments which enabled the authors to use the modified ASTM D695 test fixture. The procedure outlined in the modified ASTM D695 standard was followed for these experiments [21]. Failure was confined to the gauge region for all the specimens (shown in Fig. 2), which demonstrated that the tests were successful.

The prepared specimens were machined according to the modified ASTM D695 standard [21]. In total ten different fibre orientations were examined. The geometry of the specimen is shown in Fig. 1 and Table 1. W is the width of the specimen, T is the minimum thickness of the specimen, θ is the angle of the fibre direction relative to the loading direction, G is the length of the gauge section and L is the length of the tabs. It is important to oversize the gauge region when testing matrix failure, as this prevents the fibres extending from one tabbed region to the other. One consideration that must be noted in specimens containing tabs is that extending the gauge region implies that the specimen is more susceptible to buckling as this region is unsupported by the anti-buckling rig. In order to prevent this, the thickness of the specimens should be chosen according to Eq. (1) [22]. The material ultimate compressive strength ($F^{cu} = 610$ MPa), flexural modulus ($E^f = 131$ GPa), and interlaminar shear modulus ($G_{xz} = 4.73$ GPa) were found in another investigation by the authors [23]. The values were either provided by the material supplier [24] or obtained experimentally using ASTM D695, and ASTM D5379. A conservative design was chosen by making the steep fibre testing angles (e.g. 10–45 degrees) thicker as their designs incorporated tabs implying the support jig would not be supporting their gauge regions. Specimens with fibres positioned at angles between 50 and 90 degrees did not require tabs as they were found not to suffer from end crushing.

$$T \geqslant \frac{G}{0.9069\sqrt{\left(1-\frac{1.2F^{cu}}{G_{xz}}\right)\left(\frac{E^f}{F^{cu}}\right)}} \tag{1}$$

where T = specimen thickness, mm; G = length of gage section, mm; F^{cu} = expected ultimate compressive strength, MPa; E^f = expected flexural modulus, MPa; G_{xz} = through the thickness (interlaminar) shear modulus, MPa.

The material being used is a carbon prepreg material called EP280 Prepreg, supplied by GMS Composites [24]. Several plates of varying thickness (made according to Table 1) were laid up on aluminium plates placed on the top and bottom to maintain a flat geometry during cure. Care was taken to ensure that the fibres were aligned in the same directions. The gap between the two plates was sealed using high temperature scotch tape to prevent any resin escaping during the cure. The specimens were then cured according to the manufacturer recommendations [24] in an autoclave. A CNC was used to cut out the specimens at the desired angles. Final grinding of the sides was performed on a diamond wheel to minimise any machining defects.

Acceptable modes of failure under compression are presented in both the ASTM D 3410 and ASTM D 6641 [22,25]. They include; (a) axial splitting, (b) fibre kinking, and (c) shear failure. Global buckling is the fourth failure mode which is considered to be unsuccessful. Axial splitting and fibre kinking are typical fibre modes of failure [26]. As these experiments are examining matrix failure, the authors consider the shear failure mode to be the only acceptable behaviour.

Fig. 2 and Table 2 present the final forces at failure. It is observed that the specimens with angles between 90 and 45 degrees are found to fail suddenly with a shear mode of failure, whilst specimens with fibre angles between 30 and 10 degrees tended to slowly stop carrying load. These specimens have their fibres aligned close to the loading direction, which from Fig. 2 (h)–(j) indicate failure to have taken place due to fibre kinking. This behaviour is known to take place in 0° composites due to local instability at the fibre level when the lamina is axially loaded. Here, the elastic deformation of the fibres progresses to actual fibre fractures [26].

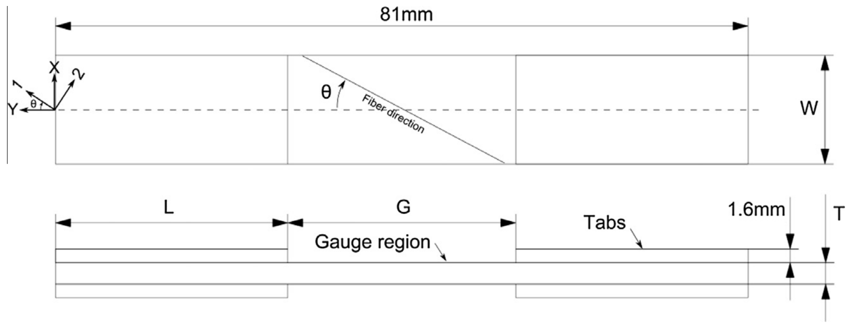

Fig. 1. Dimensions of the off-axis compression specimen.

Table 1
Dimensions of off-axis compression specimens.

Fibre angle (°)	*W* (mm)	*G* (mm)	*T* (mm)	*L* (mm)
10	6.0	41	4.75	20
20	12.7	37	4.75	22
30	12.7	23	3	29
40	12.7	17	3	32
45	12.7	17	2	32
50	12.7	81 (no tabs)	2	0 (no tabs)
60	12.7	81 (no tabs)	2	0 (no tabs)
70	12.7	81 (no tabs)	1.5	0 (no tabs)
80	12.7	81 (no tabs)	1.5	0 (no tabs)
90	12.7	81 (no tabs)	1.5	0 (no tabs)

In this study, the authors are interested in understanding the failure behaviour of matrix, which has had little attention in the past. The experiment results highlight one of the first full set of experiments performed on composites under compression for a large range of fibre orientation. Given the two distinct observations shown in Fig. 2, the specimens with fibres arranged between 90 and 45 degrees are considered successful, whilst the others are ignored for the remainder of the analysis.

2.2. Finite element analysis

Current experimental techniques are not able to distinguish stress or strain states on the matrix and fibre independently and usually stop at the lamina (global) level. Obtaining stress and strain data for the matrix requires post processing of the experimental results. This is done in a finite element analysis study. The technique separates the global stresses in the laminate to find individual stresses on the fibre and the matrix. Once the matrix stresses are obtained, they are compared against the von Mises and Drucker–Prager failure criteria [18].

One ideal method in which the failure stresses on the matrix can be obtained is to create a large analysis with each individual strand of fibre modelled, surrounded by the matrix for the entire test specimen. However using todays computing power; this is almost impossible to perform in a reasonable amount of time. The next best alternative is to extract the stress and strain state at a critical location in the global (macro) model, then impose these as boundary conditions to a unit cell. The unit cell is a Representative Volume Element (RVE) of the fibre and the matrix that can be found at the micro scale [9–11,27]. This method has started to gain popularity and is considered to be an acceptable means of establishing the micromechanical stress state in the fibre and the matrix. In order to account for the random arrangement of fibres within a lamina; the process performed on a square unit cell is repeated for a diamond and hexagonal fibre configuration. The procedure is summarised in Fig. 3.

The first stage in this approach is to obtain the stress and strain state in a global macromechanical model. Strain gauges in several experiments were used to check that the FE model gave a good prediction of this. However, a strain gauge cannot solely be used for this stage as both in-plane and out of plane stress states are required. Thus FEA aids in this process.

The stress and strain state in the centre of the specimen is found using the finite element analysis package: ABAQUS v6.13. Strain gauges were bonded onto the centre gauge region of several specimens. Classical Laminate Theory was used to model the specimen for the global macromechanical analysis. As the fibres are all arranged in the same direction, each specimen was modelled as a single lamina with material properties listed in Table 3. The FEA model was found to match the strain gauge results with a difference of less than 10%. Thus the material properties in the FE model were kept the same as those presented in Table 3. The fibre and the matrix are assumed to have isotropic properties given in Table 4 [23] which have been obtained using an inverse method of the rule of mixtures [18]. Where the lamina and matrix properties are used to obtain the fibre properties.

8-noded linear brick elements with reduced integration and hourglass control (C3D8R) were used for the micromechanical RVE models. One of the underlying conditions to enforce when performing RVE analysis is ensuring that periodic boundary conditions are maintained. This means that as the unit cell deforms, the opposing faces of the RVE must remain parallel to each other. This can be quite difficult to maintain depending on the loading conditions. For example when normal strains are applied to a unit cell shown in Fig. 3, the boundary conditions are straight forward to implement. The same case is applicable for a unit cell experiencing a pure shear load in any one of its planes. However it is difficult to combine both normal and shear loads into the same RVE analysis. This difficulty is experienced in this study, where although the main purpose of using off-axis compression specimens was to obtain a biaxial compressive stress state, significant in-plane shear stresses are also experienced due to the unbalanced specimen layup. These in-plane shear stresses need to be incorporated into the RVE analysis along with the normal strains. An approach to do this is to superimpose the results of individual RVE models [9,11,23]. This requires performing several RVE analyses (one for each load case) which can be time consuming to setup. Alternatively the authors performed a sub-modelling approach using a built in module in ABAQUS v6.13. This method passes on the strain states from the global model as displacement boundary conditions which are applied on each node of the corresponding sides of the RVE placed in the centre of the specimen. This procedure greatly shortens the time required to setup a model to perform the analysis. Fig. 4 shows the unit cell model for a square RVE before and after deformation. The unit cells were positioned in the centre of the gauge region for all the specimens as failure from the

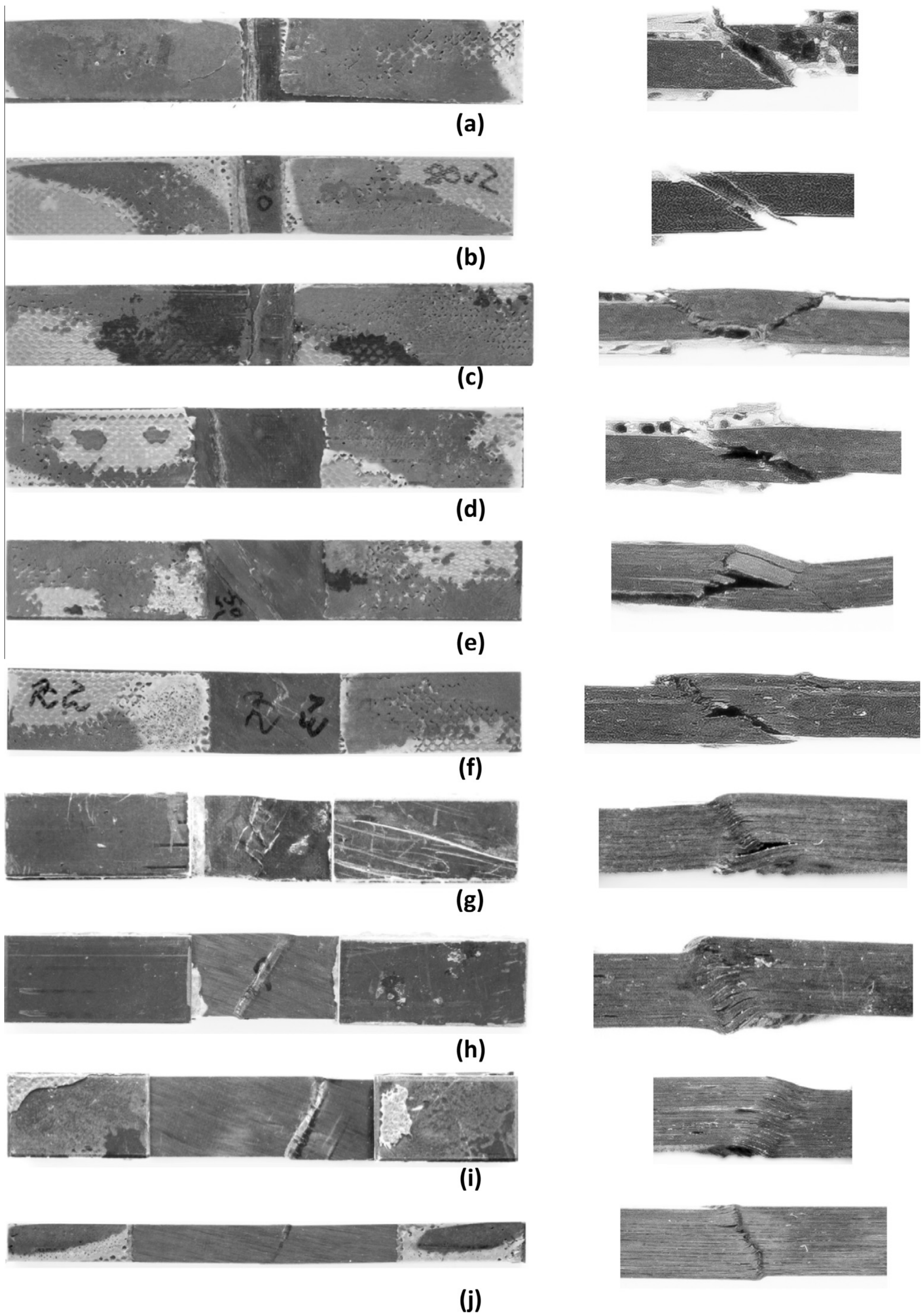

Fig. 2. Failed off-axis compression specimens. Left: top view of specimen, right: cross section of the specimen. Fibre angle: (a) 90 degrees, (b) 80 degrees, (c) 70 degrees, (d) 60 degrees, (e) 50 degrees, (f) 45 degrees, (g) 40 degrees, (h) 30 degrees, (i) 20 degrees, and (j) 10 degrees.

experiments was observed in this location (as shown in Fig. 2). Note that if failure had been observed at the corner of the tabbed regions shown in Fig. 4, more care would be needed to ensure that edge effects were correctly modelled. The deformation scale was exaggerated to observe the RVE behaviour and periodicity more easily. It was verified that the RVE shrinks in the transverse direction while expanding in the out of plane direction due to Poisson's effects. In addition to this; the RVE demonstrates in-plane shear.

2.3. Results

An advantage of the sub-modelling process is that the location of the peak stress (according to von Mises or Drucker–Prager stress criterion) can be viewed in the graphic user interface (GUI) straight away. This is far quicker than probing several locations on the model ahead of time, then superimposing stress values in order to find the critical location [9,11]. The principal stresses are recorded for each FE model and are shown in Table 5. Fig. 5 shows

Table 2
Force at failure for the off-axis compression tests.

TEST	Fibre angle (°)	Cross-sectional area (mm^2)	Force at failure (N)	TEST	Fibre angle (°)	Cross-sectional area (mm^2)	Force at failure (N)
1	90	19.05	−2495.8	15	45	25.40	−4078.78
2	90	19.05	−2778.59	16	45	25.40	−3732.22
3	90	19.05	−2047.98	17	45	25.40	−3957.02
4	80	19.05	−2740.98	18	40	38.10	−6729.77
5	80	19.05	−2216.83	19	40	38.10	−6558.68
6	80	19.05	−2413.19	20	30	38.10	−8581.61
7	70	19.05	−2431.35	21	30	38.10	−8622.96
8	70	19.05	−2639.2	22	30	38.10	−8238.75
9	70	19.05	−2415.68	23	20	60.33	−13465.36
10	60	25.40	−3545.64	24	20	60.33	−12832.83
11	60	25.40	−3489.23	25	20	60.33	−12277.63
12	50	25.40	−3216.16	26	10	28.50	−8470.27
13	50	25.40	−2713.63	27	10	28.50	−7789.31
14	50	25.40	−3452.73	28	10	28.50	−8398.7

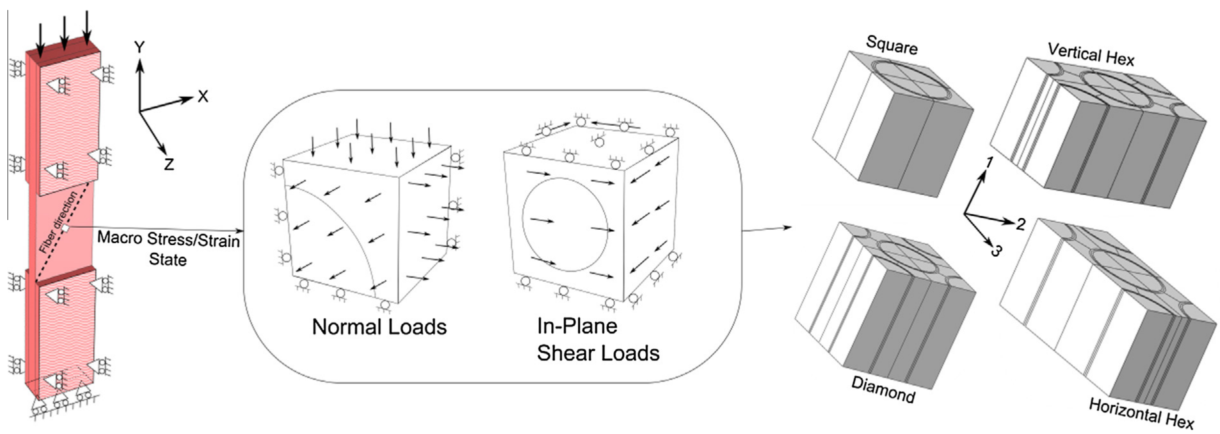

Fig. 3. RVE created in ABAQUS 6.13. (For interpretation of the references to colour in this figure legend, the reader is referred to the web version of this article.)

Table 3
Material properties of EP280 prepreg for the global macromechanical analysis.

Property	
*E*11	131 GPa
*E*22	6.20 GPa
*E*33	6.20 GPa
*v*12	0.28
*v*23	0.40
*v*13	0.28
*G*12	4.73 GPa
*G*23	1.44 GPa
*G*13	4.73 GPa

Table 4
Properties of the fibre (calculated) and matrix (from manufacturer).

Property	Fibre	Matrix
E	259 GPa	3.14 GPa
V	0.30	0.30

the critical location for the different fibre configurations in which the principal stresses were obtained. These are all taken in the mid-plane of each unit cell.

3. Uniaxial tension

From Table 5, it is evident that the matrix stress states in all the compression tests performed are in compression or shear. In this range the failure mode is distortional failure.

The testing and analysis conducted by Pipes and Gosse [14] indicated uniaxial off-axis tension tests on angles greater than 20 degrees failed in a different mode (i.e. dilatation). Thus, those angles were not tested in this paper.

3.1. Experiment methodology

Uniaxial off-axis tension tests have been performed by several authors in the past [14,28,29]. A similar test methodology was adopted to explore the failure envelope for the material used in this investigation (EP280 Prepreg).

ASTM D 3039 is used for the specimen design [30]. Fig. 6 shows the overall specimen dimensions. The use of oblique tabs has been proposed by several authors to minimising the shear stress that is introduced in such tests due to the fibre layout [31]. The oblique tabs are considered to minimise the stress concentration that takes place at the ends of the specimen during clamping. However preliminary tests showed the use of oblique tabs to cause premature failure originating from the corner of the tab rather than in the centre gauge region of the specimen. This may be due to the difficulty in aligning the oblique tabs accurately when bonding to the specimens. The authors found more success using flat tabbed specimens as suggested in the ASTM D3039. For this reason square tabs were used.

Fig. 7 shows a picture of the failed off-axis 20 degree specimen. The specimen failed just outside the end tab, which is an effect that is commonly observed with off-axis tension tests and further investigation into this phenomenon has been looked into by others [14,28,29]. The experimental data obtained from this test is shown in Table 6.

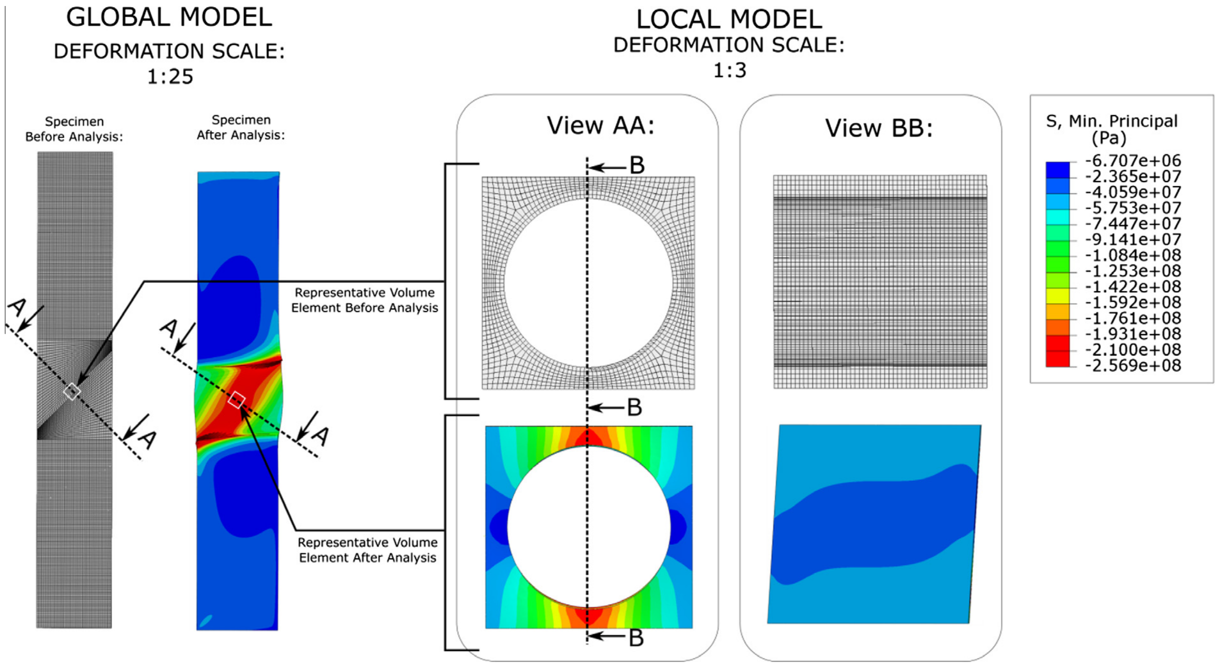

Fig. 4. Deformation of specimen and square RVE before and after the analysis (Test 15). (For interpretation of the references to colour in this figure legend, the reader is referred to the web version of this article.)

Table 5
Critical principal stresses obtained in the matrix for: uniaxial off-axis compression tests. (Stresses have been averaged based on the four fibre configurations examined.)

Test	Fibre angle (°)	σ_1 (MPa)	σ_2 (MPa)	σ_3 (MPa)	Standard deviation		
					σ_1 (MPa)	σ_2 (MPa)	σ_3 (MPa)
1	90	−77.18	−253.42	−95.60	47.27	79.26	34.96
2	90	−86.29	−281.52	−106.37	52.41	88.41	38.91
3	90	−63.60	−207.49	−78.39	38.63	65.16	28.68
4	80	−66.01	−227.05	−84.19	45.06	76.27	34.37
5	80	−55.62	−187.58	−69.57	33.86	57.41	26.06
6	80	−57.23	−195.18	−72.30	40.50	71.94	32.05
7	70	−53.06	−191.05	−67.15	31.49	58.89	27.57
8	70	−57.59	−207.38	−72.89	34.18	63.92	29.93
9	70	−52.71	−189.80	−66.72	31.29	58.51	27.40
10	60	−49.27	−198.03	−64.17	27.29	60.53	29.31
11	60	−48.49	−194.87	−63.15	26.85	59.57	28.84
12	50	−29.40	−154.37	−45.24	15.98	43.73	21.47
13	50	−24.03	−126.38	−37.12	13.57	37.92	18.49
14	50	−30.58	−160.81	−47.23	17.27	48.25	23.53
15	45	15.19	−137.00	−23.55	14.60	45.01	22.00
16	45	13.90	−125.36	−21.55	13.36	41.18	20.13
17	45	14.73	−132.91	−22.85	14.16	43.66	21.34
18	40	22.37	−134.04	−22.73	15.09	34.79	19.16
19	40	20.67	−126.11	−21.69	13.56	37.83	19.06

3.2. Processed results

The processing of the experimental results is the same as that discussed for the compression specimens in Section 2.2. The main difference is that the specimen is under a tensile load. Micromechanical analysis is also performed using the same four fibre configurations. The processed results for the matrix are shown in Table 6.

4. Discussion

This paper is mainly concerned with understanding the failure of the matrix under compression. Although the uniaxial compression tests performed would possibly have sufficed, the tension results presented in the previous section allow for a better overall understanding.

Numerous failure criteria have been proposed over the last few decades [32,33], amongst which von Mises failure criterion (Eq. (2)) is one of the most widely used due to its simplicity and ability to accurately follow experimental results. However this criterion is sometimes found to underestimate compressive failure. Drucker–Prager failure criterion is often used as an alternative. The criterion

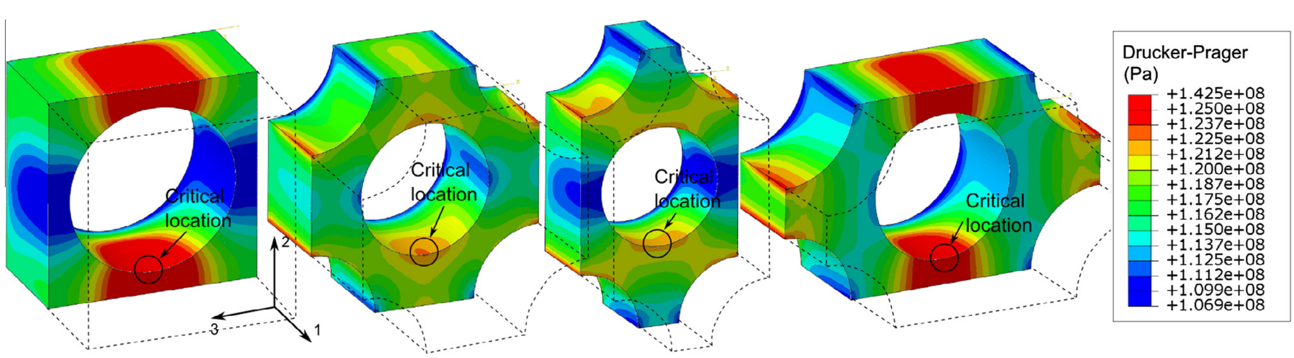

Fig. 5. Critical location for a: (a) square fibre configuration, (b) diamond fibre configuration, (c) vertical hexagonal fibre configuration, and (d) horizontal hexagonal fibre configuration. (For interpretation of the references to colour in this figure legend, the reader is referred to the web version of this article.)

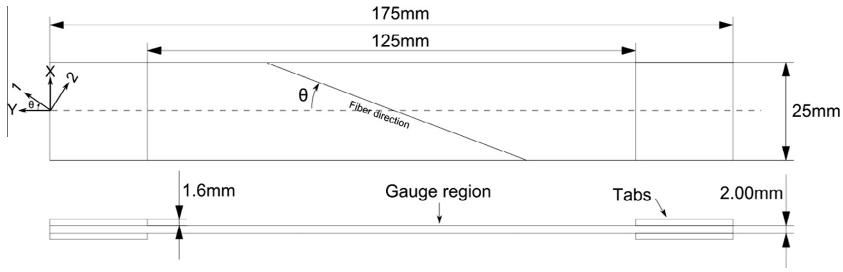

Fig. 6. Unidirectional off-axis tension specimen.

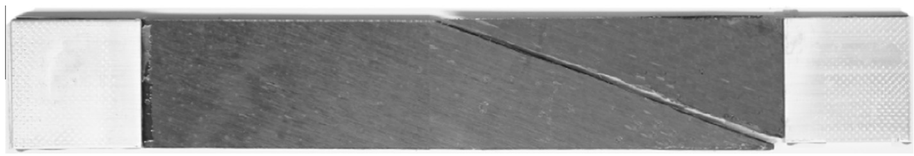

Fig. 7. Failed 20 degree off-axis tension specimen.

Table 6
Critical principal stresses & forces obtained at failure in the matrix for an off-axis 20 degree tension test. (Stresses have been averaged based on the four fibre configurations examined.)

Test	Fibre angle	Failure force (N)	σ_1 (MPa)	σ_2 (MPa)	σ_3 (MPa)	Standard deviation		
						σ_1 (MPa)	σ_2 (MPa)	σ_3 (MPa)
1	20°	9295	85.94	14.23	−35.69	48.42	4.68	31.41

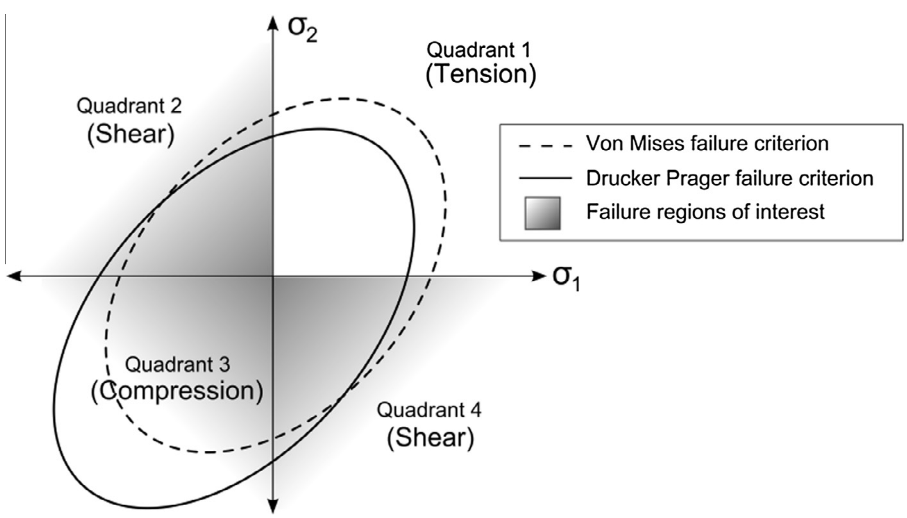

Fig. 8. An example of von Mises and Drucker–Prager failure criteria plotted in 2D Stress space.

is the same as von Mises except that it introduces another curve fitting parameter 'B' (given in Eq. (4)) to capture the hydrostatic stresses that play an important role when a material is under compression [18]. Fig. 8 shows a plot of the two failure criteria in 2D stress space. Quadrants 2, 3 and 4 shown in Fig. 8 are of interest for this investigation. A material that fails in these three quadrants is believed to fail due to distortion, which is characterised by an extensive change in the materials shape [9,12]. Quadrant 1 of the failure envelope is considered to exhibit a different behaviour characterised by dilatation, which is a change in volume of the material [3].[1] Examining this behaviour is outside of the scope for this paper and itself is an area of research that has had very limited experimental results published for the matrix.

The results here will be investigated in 3D stress space due to the significance of σ_3 shown in Tables 5 and 6. von Mises and Drucker–Prager failure criteria look like a cylinder and a cone respectively when plotted in 3D stress space.

$$\sigma_{vm} = \sqrt{3J_2} = A \tag{2}$$

where σ_{vm} is the von Mises stress, 'A' is a curve fitting parameter representing the critical stress, and J_2 is the second invariant of the deviatoric stress tensor given by Eq. (3):

$$J_2 = \frac{1}{6}\left[(\sigma_1 - \sigma_2)^2 + (\sigma_2 - \sigma_3)^2 + (\sigma_3 - \sigma_1)^2\right] \tag{3}$$

[1] The division between these two failure modes may not be exactly at the boundary between quadrant 1 and quadrant 2 (quadrant 1 and quadrant 4).

$$\sqrt{J_2} = A + BJ_1 \tag{4}$$

where J_2 is the second invariant of the deviatoric stress tensor given by Eq. (3). 'A' and 'B' are curve fitting parameters, and J_1 is the first invariant of the deviatoric stress tensor given by Eq. (5):

$$J_1 = \sigma_1 + \sigma_2 + \sigma_3 \tag{5}$$

In order to assist in the selection of a suitable failure criterion to accurately model the compressive and shear quadrants of the matrix failure envelope; six comparisons are made:

(1) Compare compression test results against the von Mises failure criterion fitted using compression test results.
(2) Compare compression results against the Drucker–Prager failure criterion fitted using compression test results.
(3) Compare compression and tension results against the von Mises failure criterion fitted using compression and tension test results.
(4) Compare compression and tension results against the Drucker–Prager failure criterion fitted using compression and tension test results.
(5) Compare compression and tension results against the von Mises criterion fitted using only compress test results
(6) Compare compression and tension results against the Drucker–Prager criterion fitted using only compress test results.

Table 7 summarises the differences in prediction given from the various regression models using the six comparisons. Eq. (6) shows the formula used for the sum of least squares analysis.

$$\mathrm{RSS} = \sum_{i=1}^{n} (y_i - f(x_i))^2 \tag{6}$$

4.1. Comparison 1

von Mises failure criterion is given by Eq. (2). It is the same as that given by Eq. (4), except that the term 'B' is equal to zero. Eq. (6) is used to calculate the residual sum of squares which is minimised by solving for values of 'A'. Eq. (7) shows the final criterion when examining only the off-axis compression results. A plot of the points on the failure criterion given by von Mises is shown in Fig. 9.

$$\sqrt{J_2} = 78.7 \tag{7}$$

4.2. Comparison 2

The same method is used to compare the Drucker–Prager criterion with the experimental results. Based on the RSS value shown in Table 7, there is an improvement in this model's ability to accurately predict the failure for the matrix material. Eq. (8) gives the final criterion obtained. Fig. 10 shows the Drucker–Prager failure criterion plotted in 3D stress space with the experimental compression results. It is evident that the criterion appears to fit the experimental results better than when a von Mises failure criterion is fitted with the RSS value decreased by 43%.

$$\sqrt{J_2} = 60.2 - 0.068J_1 \tag{8}$$

4.3. Comparison 3

The uniaxial off-axis tension result for the 20 degree specimen is now included in the regression. This is expected to increase the RSS value as another regression point is being added. However the addition of this tension results assists in examining the significance of hydrostatic stresses, allowing the selection of either the von Mises criterion or the Drucker–Prager criterion to become clearer. Eq. (9) gives the final criterion obtained. Fig. 11 shows the von Mises failure criterion plotted in 3D stress space with the experimental compression results.

$$\sqrt{J_2} = 77.8 \tag{9}$$

4.4. Comparison 4

The fourth comparison is looking at both uniaxial off-axis compression and tension results, fitting the Drucker–Prager criterion to them. From Fig. 12, it is evident that the criterion appears to fit the experimental results better than when a von Mises failure criterion is fitted. This is also shown by the RSS value which has decreased by 50%. Eq. (10) shows the parameters for 'A' and 'B' obtained from the regression analysis.

$$\sqrt{J_2} = 62.25 - 0.061J_1 \tag{10}$$

4.5. Comparison 5

The fifth comparison uses the von Mises criterion given by Eq. (7) to calculate the percentage error when the uniaxial tension result is incorporated. A plot of the results in 3D stress space is shown in Fig. 13 to aid in understanding the predictive capability of the failure criterion when examining the compressive and shear behaviours of the matrix material.

4.6. Comparison 6

The final comparison uses the Drucker–Prager criterion given by Eq. (8) to calculate the percentage error when the uniaxial tension result is incorporated. A plot of the failure envelope with the addition of the uniaxial tension result is shown in Fig. 14. This shows an improvement from comparison 5.

4.7. Selection of a failure criterion

The Drucker–Prager criterion has been shown by others to give a better representation of the failure surface for single-phased isotropic materials under compression when compared to the von Mises criterion [19,34]. This is due to its inclusion of hydrostatic stresses, which von Mises does not take into account. Despite this, there are very little experimental results to show the failure of the individual constituents in a composite. The findings presented here are one of the first to show the failure surface of the matrix when a composite lamina fails due to compression.

Using Table 7 and the six comparisons made it is evident that the Drucker–Prager criterion does a better job in explaining the compressive failure of the matrix in composites. This can be seen by comparisons: 2 and 4, where the RSS value was at least 40% lower than their counterparts: comparison 1 and 3 respectively. When Eqs. (8) and (10) are compared against each other, the value for 'A' and 'B' change slightly due to the addition of the uniaxial off-axis 20 degree tension result, however they remain relatively same in magnitude indicating that the original Drucker–Prager criterion fitted in comparison 2 did a good job in predicting failure. This becomes clearer as the RSS values given in Table 7 are looked at further.

Looking at the RSS values for comparison 4 and 6, which looks at the predictive ability of the Drucker–Prager criterion established in comparison 2, against the addition of uniaxial tension result. The RSS value is found to increases by only 1%. This small difference in

Table 7
Comparison of experimental results with the Drucker–Prager and von Mises failure criteria.

Test	Fibre angle (°)	% difference between experimental data and failure prediction found in:					
		Comparison 1	Comparison 2	Comparison 3	Comparison 4	Comparison 5	Comparison 6
Compression							
1	90	4%	7%	2%	7%	4%	7%
2	90	−5%	1%	−6%	1%	−5%	1%
3	90	4%	8%	3%	8%	4%	8%
4	80	−11%	−3%	−12%	−3%	−11%	−3%
5	80	9%	12%	7%	12%	9%	12%
6	80	4%	9%	3%	8%	4%	9%
7	70	−19%	−8%	−20%	−9%	−19%	−8%
8	70	−27%	−14%	−28%	−15%	−27%	−14%
9	70	−1%	6%	−2%	6%	−1%	6%
10	60	16%	11%	14%	12%	16%	11%
11	60	41%	31%	40%	32%	41%	31%
12	50	11%	8%	10%	8%	11%	8%
13	50	0%	−11%	−2%	−10%	0%	−11%
14	50	9%	−4%	8%	−3%	9%	−4%
15	45	3%	−9%	1%	−8%	3%	−9%
16	45	−2%	−14%	−3%	−12%	−2%	−14%
17	45	4%	−9%	3%	−7%	4%	−9%
18	40	−4%	−1%	−5%	−1%	−4%	−1%
19	40	−2%	1%	−3%	0%	−2%	1%
Tension							
1	20	–	–	27%	−5%	29%	−9%
Residual sum of squared errors (RSS):		2099	1197	2391	1213	2407	1225

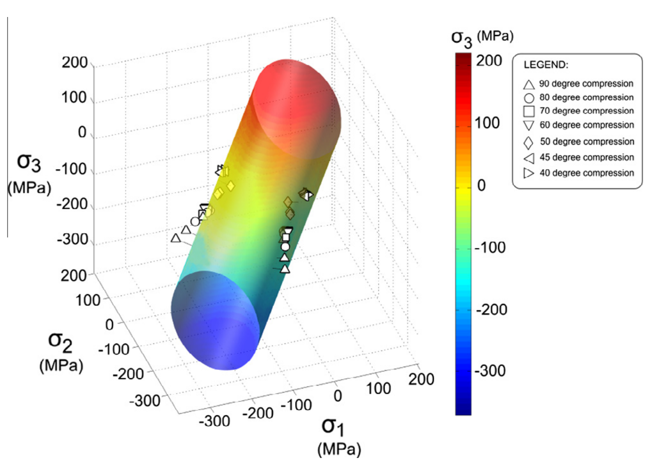

Fig. 9. Plot of uniaxial compression tests on the von Mises failure envelope. (For interpretation of the references to colour in this figure legend, the reader is referred to the web version of this article.)

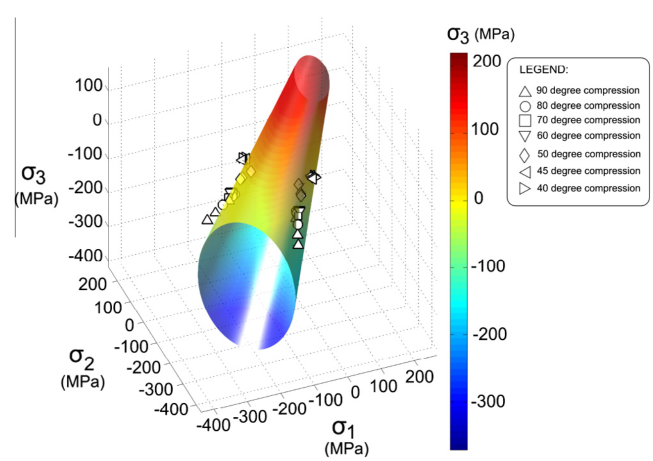

Fig. 10. Plot of uniaxial compression tests on the Drucker–Prager failure envelope. (For interpretation of the references to colour in this figure legend, the reader is referred to the web version of this article.)

error suggests that the first fit using Drucker–Prager was sufficient to capture the failure surface of the matrix, where the uniaxial tension experiments had not been performed. Thus, performing the uniaxial tension test, clarified the conical nature of the failure envelope given by Drucker–Prager in the compression and shear quadrants of the failure envelope. From these findings; Eq. (10) from comparison 4 is selected as best representing matrix failure under compression in the composite material used in this investigation.

5. Conclusions

The ASTM D695 test rig was used to perform several off-axis compression tests. In order to prevent end crushing which is an undesirable failure characteristic, it was found that the specimens with fibres positioned from 10 to 45 degrees required the use of aluminium tabs. As the centre gage region is no longer supported by the antibuckling rig, these particular specimens had their thickness increased according to Eq. (1) to prevent buckling. Following these rules allowed the collection of successful compression data. Specimens with fibre angles between 10 and 30 degrees were omitted from the remainder of the study as they were not considered to display a matrix mode of failure.

Micromechanical analysis through means of a sub-modelling approach was used in the study to separate the stress/strain state in the fibre and the matrix. As all the successful experiments indicated a matrix mode of failure, the principal stresses at a critical location of the matrix were extracted. When the results were plotted in 3D stress space it was found that the matrix was able to carry much higher loads in compression compared to when under tension. The Drucker–Prager failure criterion gave a 40% better fit to the experimental results compared to von Mises. This significant difference indicates that it is very important to consider the hydrostatic stress components when examining matrix failure under compression. The authors recommend the use of a Drucker–Prager failure criterion to model compressive/shear failure of a matrix found in composites.

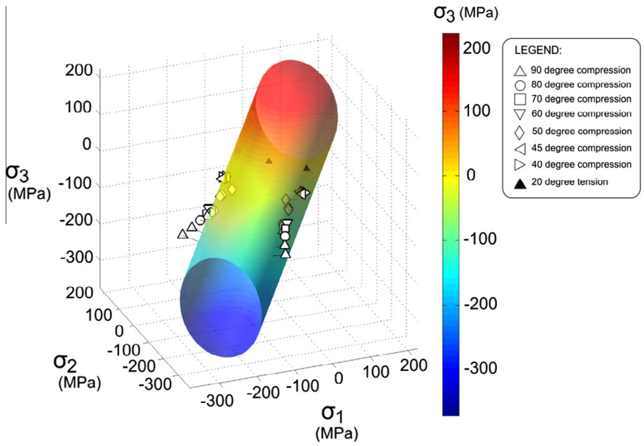

Fig. 11. Plot of uniaxial compression and uniaxial tension tests on the von Mises failure envelope. (For interpretation of the references to colour in this figure legend, the reader is referred to the web version of this article.)

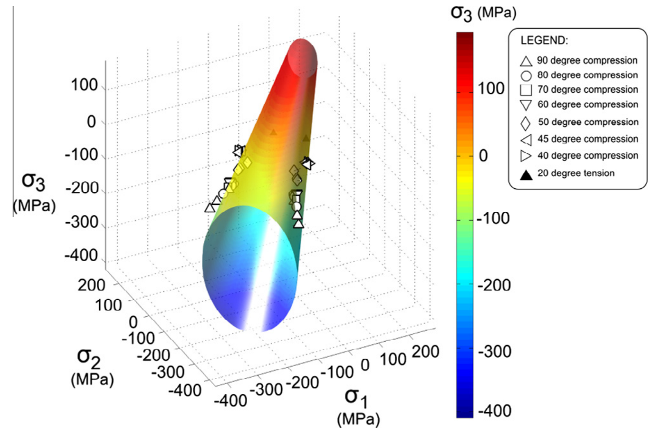

Fig. 14. Plot of uniaxial compression and uniaxial tension tests on the Drucker–Prager failure envelope fitted to only the uniaxial compression results. (For interpretation of the references to colour in this figure legend, the reader is referred to the web version of this article.)

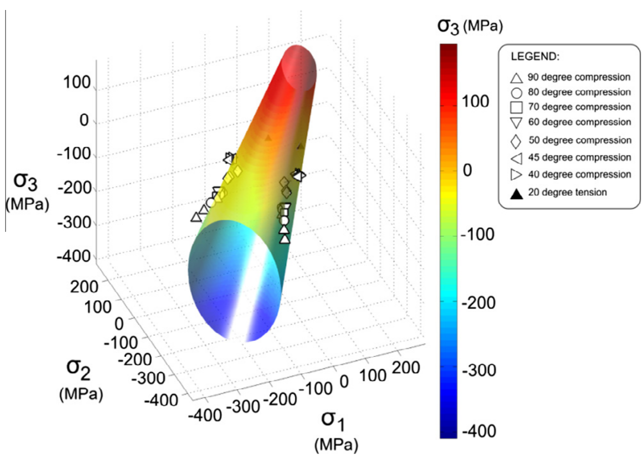

Fig. 12. Plot of uniaxial compression and uniaxial tension tests on the Drucker–Prager failure envelope. (For interpretation of the references to colour in this figure legend, the reader is referred to the web version of this article.)

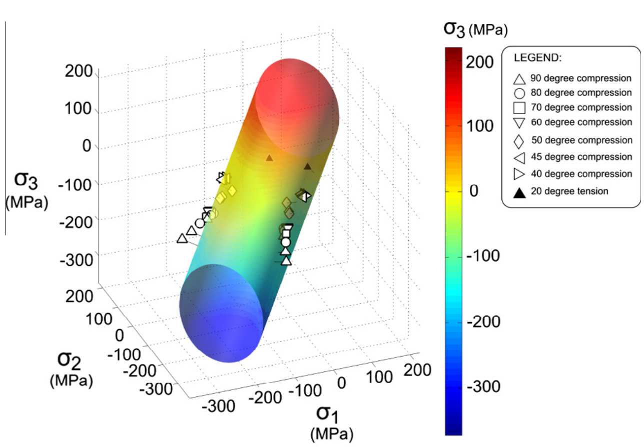

Fig. 13. Plot of uniaxial compression and uniaxial tension tests on the von Mises failure envelope fitted to only the uniaxial compression results. (For interpretation of the references to colour in this figure legend, the reader is referred to the web version of this article.)

Acknowledgements

This research was carried out partially under financial support from the Australian Defence Material Organisation and also as part of a CRC-ACS research program, established and supported under the Australian Government's Cooperative Research Centres Program.

References

[1] Jeffry W, Mayes S, Christopher K, Richard M. Comparison of MCT failure prediction techniques and experimental verification for biaxially loaded glass fabric-reinforced composite laminates. J Compos Mater 2004;38:2165–81.
[2] Reddy JN. Mechanics of laminated composite plates. CRC Press; 1997.
[3] Helius: MCT technical manual. Version 1.0 ed 2009: Firehole Technologies.
[4] Christopher TK, James L. Constituent based analysis of composite materials subjected to fire conditions. Composites: Part A 2006;37:1005–14.
[5] Shokrieh MM, Lessard LB. Progressive fatigue damage modelling of composite materials, Part II: material characterization and model verification. J Compos Mater 2000;34:1081–116.
[6] Bilel A, Michael KP, Scott WC. Progressive damage assessment of centrally notched composite specimens in fatigue. Composites: Part A 2015;74:47–59.
[7] Ireneusz L, Juan AH. Progressive damage modeling in fiber-reinforced materials. Composites: Part A 2007;38:2333–41.
[8] Kolks G, Tserpes KI. Efficient progressive damage modeling of hybrid composite/titanium bolted joints. Composites: Part A 2014;56:51–63.
[9] Hart S. Application of the strain invariant failure theory (SIFT) to metals and fibre-polymer composites. Philos Mag 2010;90:4263–331.
[10] Gosse J, Steven C. Strain invariant failure criteria for polymers in composite materials. In: AIAA structural dynamics, and materials conference; 2001. p. 45–55.
[11] Sirivedin S, Fenner ND, Nath BR, Galiotis C. Effects of inter-fibre spacing and matrix cracks on stress amplification factors in carbon-fibre/epoxy matrix composites. Part I: planar array of fibres. Composites: Part A 2003;34:1227–34.
[12] Asp L, Berglund A, Talreja R. A criterion for crack initiation in glassy polymers subjected to a composite-like stress state. Compos Sci Technol 1996;56:1291–301.
[13] Naik NK, Ganesh VK. Failure behavior of plain weave fabric laminates under in-plane shear loading. J Compos Technol Res 1994;16:3–20.
[14] Pipes RB, Gosse JH. An onset theory for irreversible deformation in composite materials. In: Proceedings of 17th international conference on composite materials (ICCM 17), 27–31 July 2009, Edinburgh.
[15] Xavier CJ, Garrido MN, Oliveira M, Morais LJ, Camanho PP, Pierron F. A comparison between the Iosipescu and off-axis shear test methods for the characterization of *Pinus Pinaster* Ait. Composites: Part A 2004;35:827–40.
[16] Chowdhury N, Chiu WK, Wang J. Biaxial specimen design for structures subjected to multi-axial loads. Adv Mater Res 2014;891:1633–8.
[17] Chowdhury N, Chiu WK, Wang J, Yan W. Comparison of failure criteria examining matrix dominant failure under biaxial loading. In: ACAM 8, 8th Australasian congress on applied mechanics; 2014.
[18] Kaw AK. Mechanics of composite materials. 2nd ed. CRC Press; 2006.
[19] Wang J, Chiu WK. Prediction of matrix failure in fibre reinforced polymer composites. J Eng 2013 973026.

[20] Orifici AC, Herszberg I, Thomson RS. Review of methodologies for composite material modelling incorporating failure. Compos Struct 2008;86:194–210.
[21] Modified ASTM D 695. Standard test method for compressive properties of rigid plastics. West Conshohocken (PA): ASTM International; 2002.
[22] ASTM D 6641. Standard test method for compressive properties of polymer matrix composite materials using a combined loading compression (CLC) test fixture. West Conshohocken (PA): ASTM International; 2009.
[23] Chowdhury N, Wang J, Chiu WK, Yan W. Predicting matrix failure in composite structures using a hybrid failure criterion. Compos Struct 2016;137:148–58.
[24] GMS composites, <http://www.gmscomposites.com/prepreg-range>.
[25] ASTM D 3410. Standard test method for compressive properties of polymer matrix composite materials with unsupported gage section by shear loading. West Conshohocken (PA): ASTM International; 2003.
[26] Leif AC, Adams DF, Pipes RB. Experimental characterization of advanced composite materials. 3rd ed. CRC Press; 2002.
[27] Okabe T, Imamura H, Sato Y, Higuchi R, Koyanagi J, Talreja R. Experimental and numerical studies of initial cracking in CFRP cross-ply laminates. Composites: Part A 2015;68:81–9.
[28] Xiao Y, Kawai M, Hatta H. An integrated method for off-axis tension and compression testing of unidirectional composites. J Compos Mater 2010;45:657–69.
[29] Sun CT, Berreth SP. A new end tab design for off-axis tension test of composite materials. J Compos Mater 1988;22:766–79.
[30] ASTM D 3039. Standard test method for tensile properties of polymer matrix composite materials. West Conshohocken (PA): ASTM International; 1995.
[31] Sun CT, Chung I. An oblique end-tab design for testing off-axis composite specimens. J Compos Mater 1992;24:619–23.
[32] Soden DP, Hinton JM, Kaddour SA. Failure criteria in fibre reinforced polymer composites: additional theories, comparison and recommendations. Spec Issue Compos Sci Technol 2004;64.
[33] Mao HY. Advances in strength theories for materials under complex stress state in the 20th century. Am Soc Mech Eng 2002;55:169–98.
[34] Wang J, Chiu WK. Enhancing prediction accuracy in sift theory. In: 18th ICCM, Jeju Island, Korea 21–26 August 2011.